Available online at www.sciencedirect.com

ScienceDirect

Advances in Space Research 67 (2021) 1049–1057

ADVANCES IN SPACE RESEARCH (a COSPAR publication)

www.elsevier.com/locate/asr

Estimation of QZSS differential code biases using QZSS/GPS combined observations from MGEX

Qisheng Wang [a,b], Shuanggen Jin [b,c,*], Youjian Hu [a,*]

[a] School of Geography and Information Engineering, China University of Geosciences, Wuhan 430074, China
[b] School of Remote Sensing and Geomatics Engineering, Nanjing University of, Information Science and Technology, Nanjing 210044, China
[c] Shanghai Astronomical Observatory, Chinese Academy of Sciences, Shanghai 200030, China

Received 27 June 2020; received in revised form 27 October 2020; accepted 29 October 2020
Available online 17 November 2020

Abstract

As an important error source in Global Navigation Satellite System (GNSS) positioning and ionospheric modeling, the differential code biases (DCB) need to be estimated accurately, e.g., the regional Quasi-Zenith satellite system (QZSS). In this paper, the DCB of QZSS is estimated by adopting the global ionospheric modeling method based on QZSS/GPS combined observations from Multi-GNSS experiment (MGEX). The performance of QZSS satellite and receiver DCB is analyzed with observations from day of year (DOY) 275–364, 2018. Good agreement between our estimated QZSS satellite DCB and the products from DLR and CAS is obtained. The bias and root mean square (RMS) of DCB are mostly within ±0.3 ns. The day-to-day fluctuation of the DCB time series is less than 0.5 ns with about 96% of the cases for all satellites. However, the receiver DCB is a little less stable than satellite DCB, and their standard deviations (STDs) are within 1.9 ns. The result shows that the stability of the receiver DCBs is not significantly related to the types of receiver or antenna.

Keywords: Quasi-Zenith satellite system (QZSS); GPS; Differential code biases (DCB); Multi-GNSS experiment (MGEX)

1. Introduction

Japan's Quasi-Zenith satellite system (QZSS) is a regional system that can provide services in the Asian Pacific region. Several QZSS satellites have been launched since 2010. The initial service has been offered by the current QZSS constellation, which contains only 4 satellites (Li et al. 2019c). The Japanese Cabinet Office published the announcement that 7 satellites were under development for establishing the second phase of QZSS (Zhang et al. 2018). This system will be finished by 2024. Many researchers have been investigating the satellite attitude, signal analysis and orbit determination as well as positioning performance of QZSS (Hauschild et al., 2011; Li et al., 2019c; Odolinski et al., 2014; Quan et al., 2015; Zhang et al., 2018). With the rapid expansion of the QZSS system, QZSS will play a more important role in the future Global Navigation Satellite System (GNSS) constellations (Zhang et al. 2018).

As an important error source in GNSS precise point positioning (PPP) and ionospheric modeling, the differential code biases (DCB) needs to be estimated accurately and correctly (Jin et al., 2012; Jin and Su, 2020). The DCB estimation can be categorized into the following three methods. In the first method, the DCB and ionospheric total electronic content (TEC) parameters are estimated together in the ionosphere model (Jin et al., 2012; Xue

* Corresponding authors at: School of Remote Sensing and Geomatics Engineering, Nanjing University of, Information Science and Technology, Nanjing 210044, China (S. Jin). School of Geography and Information Engineering, China University of Geosciences, Wuhan 430074, China (Y. Hu).

E-mail addresses: wangqisheng0702@163.com (Q. Wang), sgjin@nuist.edu.cn, sg.jin@yahoo.com (S. Jin), hyj_06@163.com (Y. Hu).

https://doi.org/10.1016/j.asr.2020.10.049
0273-1177/

et al., 2016b; Zhang and Zhao, 2018). This method has been well established for generating global ionosphere maps and DCB products of GPS and GLONASS by some International GNSS Service (IGS) analysis centers, such as the Center for Orbit Determination in Europe(CODE) and European Space Agency(ESA) as well as Wuhan University(WHU) (Zhang and Zhao 2018). Furthermore, Li et al. (2012) proposed a new method called IGG based on single station ionospheric modeling. Then, the IGG (Institute of Geodesy and Geophysics, CAS) method was adopted by the Chinese Academy of Science (CAS) to generate the DCB products of multi-GNSS (Wang et al. 2016). In the second method, TEC calculated from the global ionospheric map (GIM) is used as compensation for ionospheric delays. The corrected observations are then applied to the estimation of the satellite DCBs. German Aerospace Center (DLR) estimates multi-GNSS DCBs by using this method (Montenbruck et al. 2014a). Moreover, uncombined precise point positioning (UPPP) technology has caused widespread concern during the last years. Another method is to calculate the ionospheric delay and DCB based on dual-frequency UPPP (Fan et al., 2017; Liu et al., 2019; Shi et al., 2015; Zhang, 2012).

There are many studies on DCB of GPS and GLONASS in the research literature (Jin et al., 2012; Li et al., 2017b; Lin et al., 2014; Sanz et al., 2017; Zhang and Zhao, 2018; Zhang et al., 2017). The GPS DCB is generally considered to be relatively stable due to its widely distributed stations and higher quality of observations (Wang et al., 2016; Zhang and Zhao, 2018). However, the stability of GLONASS DCB is worse than that of GPS DCB because of its signal adopting frequency division multiple access (FDMA) technology (Zhang et al. 2017). Besides, the Galileo DCB was also analyzed in detail by Li et al. (2017a). With the rapid development of BDS, the estimation and analysis of BDS DCB have been carried out by many researchers(Fan et al., 2017; Jin et al., 2016; Li et al., 2017b, 2019b, 2014, 2012; Shi et al., 2015; Xue et al., 2016b). Since QZSS, with four satellites in orbit began to provide regional services in 2018, a good opportunity to analyze the performance of QZSS is provided. Although the same frequency signals as GPS are used in QZSS, the satellite orbits and service coverage area of QZSS are different from GPS. Therefore, as a part of a GNSS constellation, the DCB of QZSS also needs to be estimated and analyzed.

Currently, six types of code observations can be tracked by QZSS satellites, which include C1X, C2X, and C5X as well as C1C, C2L, and C5Q. Therefore, four types of DCB for QZSS need to be estimated (eg.C1X-C2X, C1X-C5X, C1C-C2L, and C1C-C5Q). With the development of the Multi-GNSS Experiment (MGEX) network, more and more stations are available for the tracking of Multi-GNSS satellites (Montenbruck et al., 2014b, 2017). However, stations tracking QZSS satellites are mostly distributed in the Asia Pacific region. It is not feasible to model GIM and estimate DCB simultaneously based on QZSS. In this paper, we take an approach by modeling the GIM and estimating DCB simultaneously based on QZSS/GPS combined observations. The C1C-C2W DCB of GPS and four types of DCB for QZSS as well as the ionospheric TEC parameters are estimated with the method.

This paper is organized as follows: In Section 2, we describe the MGEX observations and DCB estimation methods. In Section 3, the DCB estimation method is validated by the comparison of our estimated GIM and GPS DCB with the corresponding products provided by IGS. Furthermore, the QZSS satellite and receiver DCB are estimated and analyzed by using the MGEX observations from DOY 275 to DOY 364, 2018. The conclusions and summarization are presented in Section 4.

2. Data description and methodology

2.1. MGEX observations

Observations from about 250 stations of the MGEX network were collected for estimating the QZSS satellite and receiver DCBs. The period of data covered 90 days, from DOY 275–364. During the period, solar flux conditions were quietly with about 70 flux units. Fig. 1 shows the distribution of MGEX stations and sub-trajectories of QZSS satellites. All of the selected MGEX stations support the tracking of GPS satellites, and only a few stations can track the QZSS satellites. Fig. 1 shows the sub-trajectories of QZSS satellites (red, blue, cyan and magenta lines) mainly cover the Asian-Pacific region, and the stations that support the tracking of QZSS satellites (red triangles) are also mainly distributed in the Asia-Pacific region. Therefore, we estimate the ionosphere TEC and DCB by combining GPS and QZSS observations. In this

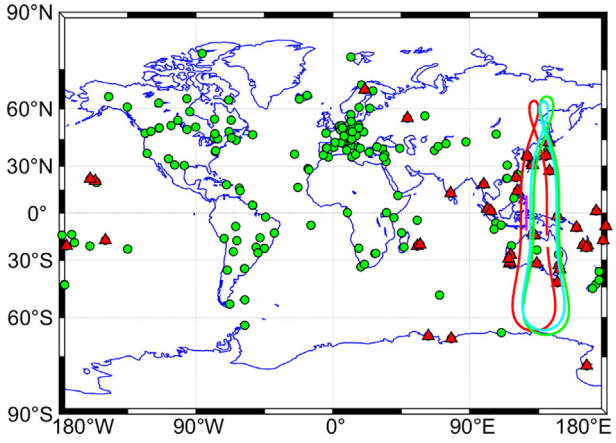

Fig. 1. Distribution of MGEX QZSS and GPS tracking stations. Red triangles represent the stations support the tracking of both QZSS and GPS satellites, green circles represent the stations support the tracking of GPS satellites. The red, blue, cyan and magenta lines represent the sub-trajectories of QZSS satellites, respectively. (For interpretation of the references to colour in this figure legend, the reader is referred to the web version of this article.)

study, GPS C1C and C2W observations from approximately 250 selected stations, QZSS C1X, C2X, and C5X observations from 30 selected stations, as well as QZSS C1C, C2L, and C5Q observations from 20 selected stations were processed. Table 1 lists the details of 50 QZSS tracking stations.

2.2. DCB estimation method

Pseudo-range and carrier phase measurements are the common types of observation for the GNSS receiver. With the consideration of many error sources, pseudo-range and carrier phase observation equations can be expressed as (Jin et al., 2012; Zhang et al., 2017):

$$\begin{cases} P_{k,j}^{s,i} = \rho_j^i + d_{ion,k,j}^i + d_{trop,j}^i + c\left(\tau^i - \tau_j\right) + d_k^i + d_{k,j} + \varepsilon_{P,k,j}^i \\ L_{k,j}^{s,i} = \rho_j^i - d_{ion,k,j}^i + d_{trop,j}^i + c\left(\tau^i - \tau_j\right) - \lambda\left(b_{k,j}^i + N_{k,j}^i\right) + \varepsilon_{L,k,j}^i \end{cases} \tag{1}$$

where, P and L represent the GNSS pseudo-range and carrier phase observations, respectively; S refers to the GNSS constellation type (here G for GPS and J for QZSS); i and j refer to the satellite and stations, respectively; k refers to the frequency, ρ represents the geometric range between the satellite and the station; d_{ion} and d_{trop} represent the ionosphere delay and troposphere delay, respectively; c is the speed of light in vacuum; τ^i and τ_j represent the satellite clock error and receiver clock error, respectively; d_k^i and $d_{k,j}$ are the code delays at frequency f_k for satellite and receiver, respectively; λ refers to wavelength; $b_{k,j}^i$ represents the uncalibrated phase delays of the satellite and the receiver. $N_{k,j}^i$ represents the ambiguity; ε_P and ε_L represent the noises of pseudo-range and carrier phase observations, respectively.

In the case of dual-frequency observations, GPS and QZSS ionospheric delays can be obtained with the geometry-free observations (Li et al., 2019b; Zhang et al., 2017):

$$\begin{cases} P_4^G = P_{1,j}^i - P_{2,j}^i = \left(d_{ion,1,j}^i - d_{ion,2,j}^i\right) + DCB^i + DCB_j \\ P_4^J = P_{1,j}^i - P_{2,j}^i = \left(d_{ion,1,j}^i - d_{ion,2,j}^i\right) + DCB^i + DCB_j \end{cases} \tag{2}$$

where $DCB^i = d_1^i - d_2^i$, and $DCB_j = d_{1,j} - d_{2,j}$; P_4^G and P_4^J represent the geometry-free observations of GPS and QZSS, respectively. A carrier phase smoothing pseudo-range is adopted to reduce the P_4 noise. When ignoring the higher-order effects of the ionosphere delays, the slant TEC (STEC) can be obtained as follows:

$$\begin{cases} \tilde{P}_4^G = 40.3\left(\frac{1}{f_{G,1}^2} - \frac{1}{f_{G,2}^2}\right) STEC_j^i + DCB_G^i + DCB_{G,j} \\ \tilde{P}_4^J = 40.3\left(\frac{1}{f_{J,1}^2} - \frac{1}{f_{J,2}^2}\right) STEC_j^i + DCB_J^i + DCB_{J,j} \end{cases} \tag{3}$$

where is the slant total electron content in the signal propagation path between GNSS satellites and ground receivers; STEC can be converted to vertical TEC (VTEC) by using the single layer mapping function. Generally, the spherical harmonic function is widely used in ionosphere modeling. The corresponding expression can be defined as (Zhang and Zhao, 2018; Zhang et al., 2017):

Table 1
Observation type, QZSS receiver and antenna brand and mode, as well as the name of stations selected for estimating DCB.

Observation type	Receiver type	Antenna type	Station
C1X, C2X, C5X	JAVAD TRE_3 DELTA	JAVRINGANT_DM	ARHT
	JAVADTRE_G3TH DELTA	JAVRINGANT_DM	HAL1
		ASH701945G_M	KOKV
	TRIMBLE NETR9	ASH701945C_M	PARK
		JAVRINGANT_DM	SOLO,TUVA,LAUT, ANMG,NCKU
		JAV_GRANT-G3T	CMUM
		LEIAR25.R3	KIR8,SIN1
		TRM55971.00	REUN,KOUC, LPIL,NMEA,NRMD
		TRM59800.00	TSK2,KIRI,PNGM,MRO1
			AIRA,STK2,DAE2,CCJ2, GMSD,CUT0,ISHI,KZN2, DAEJ
C1C,C2L,C5Q	SEPT POLARX4	SEPCHOKE_MC	KIRU, NNOR
		LEIAR25.R4	FAA1
	SEPT POLARX5	AOAD/M_T	MAW1,TID1,CEDU,HOB2
		ASH701945C_M	STR1
		ASH701945E_M	IISC
		JAVRINGANT_DM	VACS,DARW
		LEIAR25	YAR3
		LEIAR25.R3	DAV1, KAT1
		LEIAT504	YARR
		TRM57971.00	NRMG
		TRM59800.00	TONG,PTGG
	SEPT POLARX5TR	LEIAR25.R4	GAMG
	TRIMBLE NETR9	JAVRINGANT_DM	LAUT

$$\begin{cases} VTEC(\beta,s)=\sum_{n=0}^{n_{\max}}\sum_{m=0}^{n}\tilde{P}_{nm}(\sin\beta)(a_{nm}\cos ms+b_{nm}\sin ms) \\ VTEC=STEC/M(z) \\ M(z)=\frac{1}{\cos z'},\ \sin z'=\frac{R}{R+H}\sin z \end{cases} \tag{4}$$

where R is the average radius of the Earth; $H = 450$ km is the assumed single-layer ionosphere height; z and z' are the satellite zenith angle between the receiver and the corresponding ionosphere pierce point (IPP), respectively;$M(z)$ is the single layer mapping function; β and s refer to the latitude and longitude of IPPs. Note that there are calculation errors in the extraction of ionospheric measurements(Li et al. 2019a). Here, we do not consider the calibration errors, and a 20°cutoff elevation angle is set to mitigate multipath errors.

Based on the combination of Eq. (3) and Eq. (4), the unknown parameters that need to be estimated are the coefficients of spherical harmonic function and the satellite and receiver DCBs of GPS and QZSS. The order of the spherical harmonic function is set to 15 and the coefficients of the spherical harmonic function are estimated every 2 h. The satellite and receiver DCBs of GPS and QZSS are estimated as one constant in an entire day, respectively (Xue et al. 2016b). Due to the correlation between satellite and receiver DCB, the zero-mean condition on satellite DCBs is adopted. Moreover, considering the continuity between the consecutive sets of the spherical harmonic coefficient, a piecewise linear (PWL) interpolation strategy is adopted in our estimation. Thus, in our estimated DCB parameters, the type of GPS DCB is C1C-C2W, and the types of QZSS DCBs are C1X-C5X and C1X-C2X as well as C1C-C2L and C1C-C5Q.

3. Results and analysis

3.1. Method validation

In this study, the GPS and QZSS observations from MGEX can estimate ionospheric TEC and GPS C1C-C2W DCB as well as QZSS DCB simultaneously. In order to validate the method, the GIM provided by CODE is used as a reference. Since the combined GPS and GLONASS observations are used in CODE, in which the daily GIM is generated by three consecutive days of data. However, the GLONASS observations are not used in our study, and the QZSS observations can only be tracked in the Asia Pacific region. Moreover, the observations used in the study are collected from MGEX, while the data used by CODE comes from IGS. Thus, there is a bias between our estimated VTEC and CODE's VTEC. The bias and RMS of our estimated global VTEC with respect to those from CODE are presented in Fig. 2. As can be seen, the mean bias is about 1.5 TECu and the mean RMS is about 2.8TECu. Similarly results also was reported by Xue et al. (2016a), in which a mean bias of 1.54TECu can be found between they estimated GIM by using MGEX observations and the GIM from IGS. During the DOY 275–292, the mean Bias and RMS show a larger value, which may be caused by fewer available observations, since greater quantities of available observations are helpful to improve the precision of the least square adjustment results. Similarly, the GPS C1C-C2W DCB provided by DLR and CAS is used as a reference. The bias and RMS of our estimated GPS C1C-C2W satellite DCB with respect to those from DLR and CAS are presented in Fig. 3. The bias and RMS are mostly less than 0.2 ns, and the mean RMS are 0.13 and 0.12 ns, with respect to the DLR and CAS, respectively. Our estimated GPS C1C-C2W satellites DCB shows good agreement with DLR and CAS. The results of Fig. 2 and Fig. 3 evidently indicate that the proposed method in this study can be used for high precision DCB estimation.

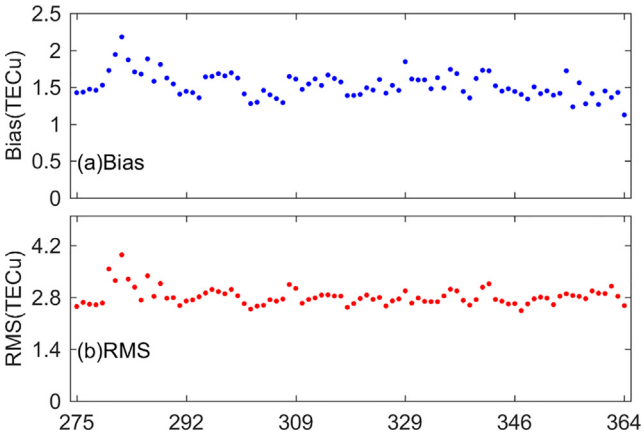

Fig. 2. The Bias and RMS of our estimated VTEC with respect to the products provided by CODE. Subplot (a) Bias, (b) RMS.

3.2. QZSS satellite DCBs

90 days DCBs have been estimated for analyzing the stability of QZSS satellites' DCBs. Fig. 4 presents the esti-

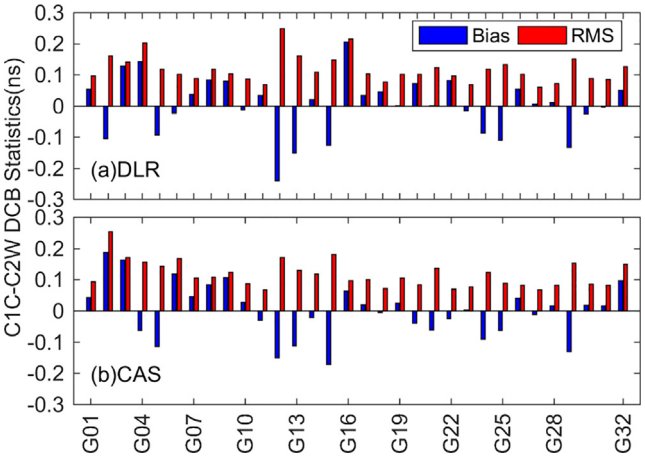

Fig. 3. The Bias and RMS of our estimated GPS C1C-C2W satellites DCB with respect to the products provided by DLR (Subplot (a)) and CAS (Subplot (b)).

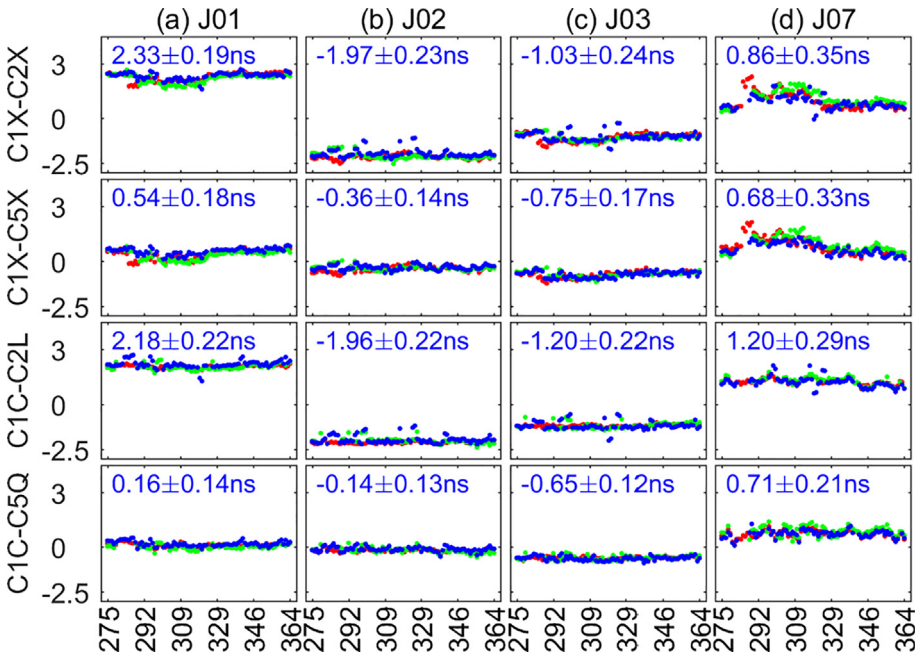

Fig. 4. Time series of our estimated QZSS satellites DCB and products provided by DLR and CAS. The blue, red and green lines represent our estimated DCB, DLR, and CAS, respectively. Subplot (a) J01 satellite, (b) J02 satellite, (c) J04 satellite, (a) J07 satellite. (For interpretation of the references to colour in this figure legend, the reader is referred to the web version of this article.)

mated QZSS DCB and those from the DLR and CAS, which are treated as a reference in this study. The good agreement between estimated QZSS satellite DCBs and those form DLR and CAS is shown. The DCB values of QZSS satellites vary within ±3 ns. The mean value and STD of satellite DCBs are plotted in Fig. 4 (where 2.33 ± 0.19 ns represents that the mean value and STD of satellite DCB are 2.33 and 0.19 ns, respectively). It can be seen that the stability of the J07 satellite DCB is obviously worse than that of other satellites, which is due to the J07 observations being tracked over a short period. Moreover, Fig. 4 shows some satellite DCBs have evident jumps, which are caused by observations omitted on those specific days. Take C1X-C2X DCB for an example. If the J01 satellite has no observations, the DCB of other satellites will cause a fluctuation of about 0.8 ns, because the DCB value of the J01 satellite is about 2.33 ns, larger than that of other satellites. Thus, there are obvious jumps in the C1X-C2X DCB time series of the other three satellites. Similarly, this phenomenon occurred in the C1C-C2L DCB time series of some satellites due to the same reason. However, the obvious jumps are not found in C1X-C5X and C1C-C5Q DCB time series, because the values of these two types of DCBs for all satellites are less than 0.8 ns, the fluctuation of DCB for other satellites is less than 0.3 ns due to the absence of observations from one satellite. Therefore, the maximum fluctuations of the two types of DCBs, C1X-C2X, and C1C-C2L, are larger than those of the other two types. The maximum fluctuations of QZSS satellite DCB are shown in Fig. 5. Table 2 presents the mean STD of estimated satellite DCB, and those from DLR and CAS. The mean STD of estimated DCB and those from DLR and CAS are 0.21, 0.18, and 0.24 ns, respectively. It indicates that the stability levels of our estimated DCB and DLR, as well as CAS, are the same.

Fig. 6 presents the histograms of day-to-day variations of our estimated QZSS satellites DCB, where 'max' and 'min' labels in each subplot shows the max and min

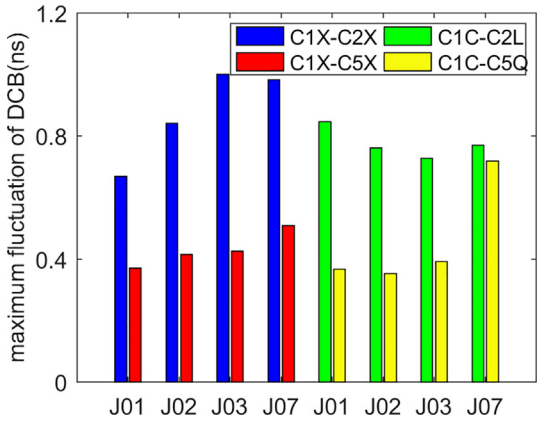

Fig. 5. Maximum fluctuation of QZSS satellites DCBs.

Table 2
Mean STD of satellites DCB of our estimated DCB, DLR, and CAS.

Type	Our estimated	DLR	CAS
C1X-C2X	0.2507	0.2699	0.3081
C1X-C5X	0.1944	0.2362	0.2776
C1C-C2L	0.2257	0.0893	0.1753
C1C-C5Q	0.1691	0.1244	0.1919
Mean	0.2100	0.1800	0.2382

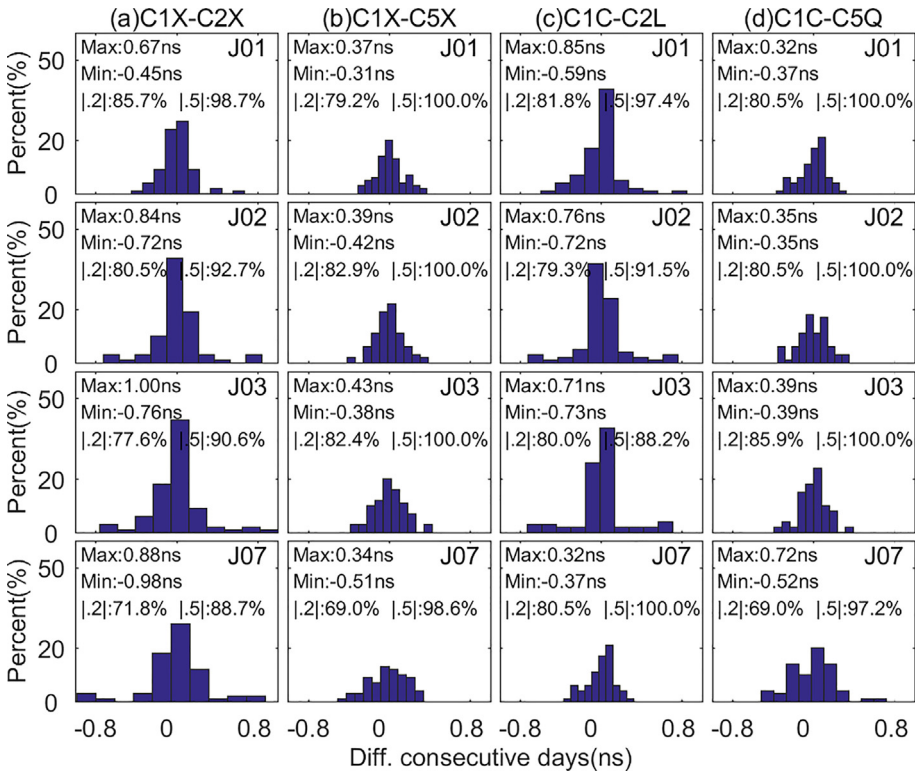

Fig. 6. Histograms of day-to-day variations of our estimated QZSS satellites DCB. Subplot (a) C1X-C2X, (b) C1X-C5X, (c) C1C-C2L, (d) C1C-C5Q.

fluctuation in DCB time series of 90 days, |0.2| and |0.5| represent the percentage of the absolute value of fluctuations in DCB time series is less than 0.2 ns and less than 0.5 ns, respectively. It can be seen that the fluctuation in the DCB time series is less than 0.5 ns with about 96% of the cases for all satellites. Moreover, for all satellites and all days, the fluctuation in the DCB time series is less than 0.2 ns in about 80%. However, some fluctuations show larger values (i.e., >0.8 ns) in the C1X-C2X and C1C-C2L DCB time series, which is related to the larger jumps of other satellites caused by some missing satellites. It can be concluded that the fluctuation of QZSS satellite DCB is mostly within 0.5 ns.

Fig. 7 shows the bias and RMS of estimated QZSS satellites DCB with respect to the products provided by DLR and CAS. The Bias and RMS of DCB with respect to DLR are mostly within 0.2 ns; and the values with respect to CAS are mostly less than 0.3 ns. It is clear that the RMS of the J07 satellite DCB shows larger values than other satellites, which may be related to fewer observations of the J07 satellite. Table 3 gives the mean Bias and RMS of estimated satellite DCBs, compared to the reference form DLR and CAS. It can be seen that our estimated QZSS satellites DCB shows a good agreement with the DCB of DLR and CAS. The mean RMS of DCB with respect to DLR and CAS are about 0.14 ns and 0.17 ns, respectively. It indicates that our estimated DCB can achieve high accuracy.

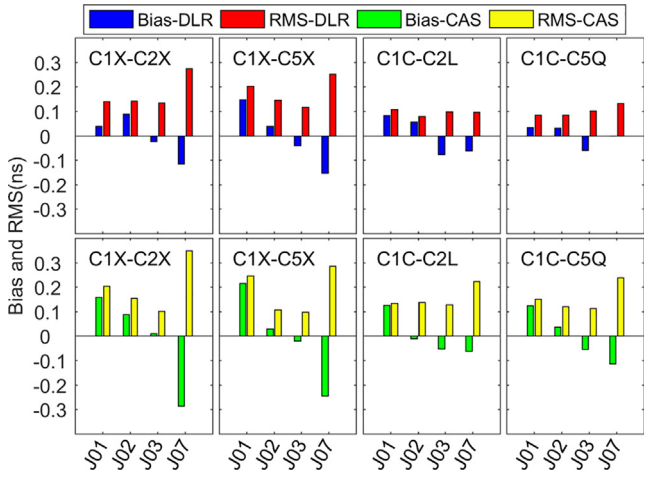

Fig. 7. The Bias and RMS of our estimated QZSS satellites DCB with respect to the products provided by DLR and CAS.

Table 3
Mean Bias and RMS of satellites DCB with respect to DLR and CAS.

Type	DLR		CAS	
	Bias	RMS	Bias	RMS
C1X-C2X	−0.0022	0.1723	−0.0077	0.2026
C1X-C5X	−0.0021	0.1785	−0.0049	0.1839
C1C-C2L	−0.0003	0.0952	0.0002	0.1555
C1C-C5Q	0.0006	0.1007	−0.0010	0.1559
Mean	−0.0010	0.1367	−0.0033	0.1745

3.3. QZSS receiver DCBs

In this study, data at 50 stations of the MGEX network were collected to estimate the DCB of QZSS. Among them, 30 stations that can track the C1X, C2X, and C5X code observations, and another 20 stations can track the C1C, C2L, and C5Q code observations. Fig. 8 shows the time series of our estimated QZSS receiver DCBs. The four subplots in Fig. 8 have the same y-axis scale. The trends of C1X-C2X and C1X-C5X receiver DCBs are similar within the period of DOY 275–364, 2018. This is also shown for C1C-C2L and C1C-C5Q receiver DCB. A comparison of Fig. 4 with Fig. 8 shows that the fluctuation of the receiver DCB is obviously larger than that of the satellite DCB. This means the receiver DCB is not as stable as the satellite DCBs.

Fig. 9 presents the mean values and STDs of our estimated QZSS receivers DCB. The stations are arranged according to the type of receiver and antenna, which are listed in Table 1. Table 4 shows the statistics for STD of the receivers DCBs. As can be seen from Fig. 9 and Table 4, the STD of all receivers DCB are less than 1.9 ns. The mean STD of C1X-C2X and C1X-C5X receiver DCBs are 0.61 and 0.64 ns, respectively. The value for C1C-C2L and C1C-C5Q receiver DCBs are 0.62 and 0.65 ns, respectively. For the stations with the same type of receiver and antenna, the mean of their C1X-C2X or C1X-C5X receiver DCB are closer. However, this phenomenon is not so obvious in the C1C-C2L and C1C-C5Q receiver DCBs. It is related to fewer stations with the same receiver type and the same antenna type (Table 1). Note that the stability of receiver DCB is affected by some factors including the receiver type, antenna type and firmware version, as well as the receiver environment (Li et al., 2017a; Xue et al., 2016b; Zhang and Teunissen, 2015). However, this

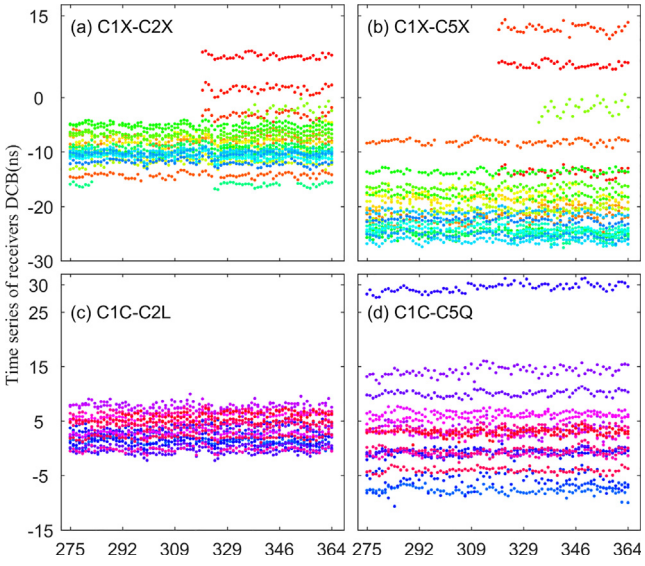

Fig. 8. Time series of our estimated QZSS receivers DCB. Subplot (a) C1X-C2X, (b) C1X-C5X, (c) C1C-C2L, (d) C1C-C5Q.

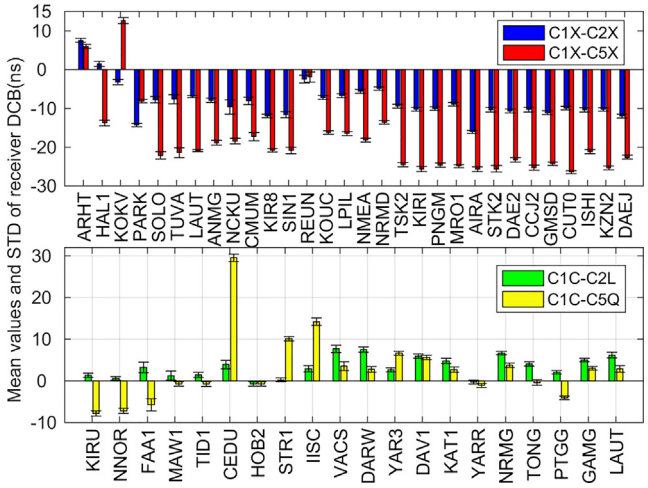

Fig. 9. Mean values and STDs of our estimated QZSS receivers DCB.

Table 4
Statistics for STD of receivers DCB.

Type	Mean	Max	Min
C1X-C2X	0.6113	1.8281	0.3111
C1X-C5X	0.6425	1.2894	0.2844
C1C-C2L	0.6203	1.2370	0.4211
C1C-C5Q	0.6475	1.4454	0.3464

information related to the receiver environment is lacking in this study, and the relationship between the stability of the receiver and the receiver environment is not discussed. Moreover, during the period of this study, there is no change in the receiver firmware version. The following analysis mainly focuses on the receiver type and antenna type. To further study the relationship between the receiver stability and type of receiver and antenna, Tables 5 and 6 show the statistics for some QZSS receiver DCBs with the same receiver and antenna type. It is can be seen that the STD of receiver DCB shows different values. In other words, the stability of the receiver DCB may not be significantly related to the type of receiver and antenna. Moreover, Fig. 10 shows the STDs of our estimated QZSS receiver DCBs and the stations are aligned by geomagnetic latitudes at the horizontal axis. It can be seen that the stability of receiver DCBs has a significant relationship with geomagnetic latitudes. Since the ionosphere in the low-

Table 5
Statistics for some QZSS receiver DCB with SEPT POLARX5 receiver and JAVRINGANT_DM antenna (ns).

Station	C1X-C2X		C1X-C5X	
	Mean	STD	Mean	STD
SOLO	−7.7729	0.8398	−22.0762	0.9252
TUVA	−7.6344	1.1459	−21.3852	1.2848
LAUT	−6.9513	0.3111	−20.8868	0.2844
ANMG	−7.8854	0.5569	−18.8488	0.6403
NCKU	−9.6406	1.8281	−18.4016	0.7144

Table 6
Statistics for some QZSS receiver DCB with TRIMBLE NETR9 receiver and AOAD/M_T antenna (ns).

Station	C1C-C2L		C1C-C5Q	
	Mean	STD	Mean	STD
MAW1	1.2837	1.0589	−0.7223	0.5445
TID1	1.4086	0.6387	−0.7596	0.5777
CEDU	3.8938	0.9620	29.5171	0.9036
HOB2	−0.7378	0.4972	−0.7483	0.5380

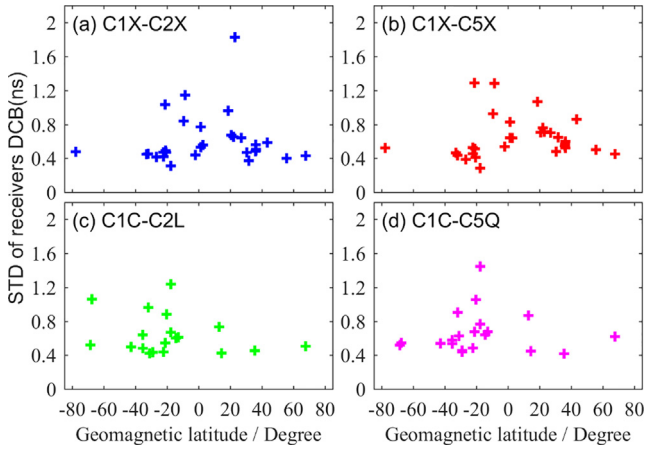

Fig. 10. STDs of our estimated QZSS receivers DCB and the stations are aligned by geomagnetic latitudes at the horizontal axis. Subplot (a) C1X-C2X, (b) C1X-C5X, (c) C1C-C2L, (d) C1C-C5Q.

latitude area is active and the accuracy of the ionosphere modeling is also poor.

Fig. 11 presents the RMS of our estimated some receivers DCB with respect to the products provided by DLR and CAS and Table 7 lists statistics for RMS. As can be seen, the values of RMS are mostly less than 1 ns, and the RMS of receiver DCBs with respect to DLR is smaller than that with respect to CAS. The RMS of our estimated

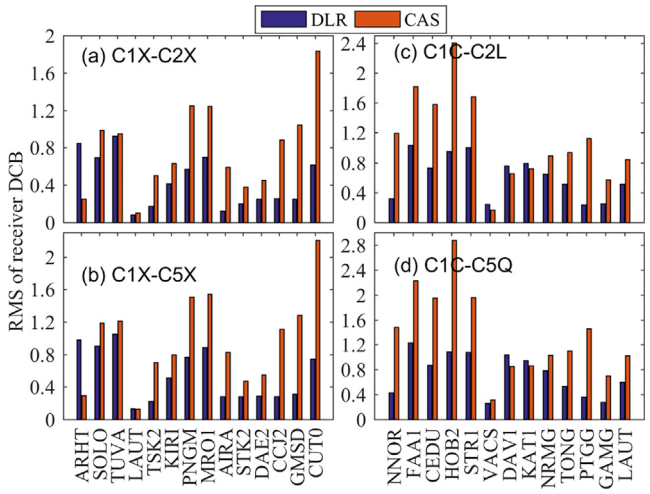

Fig. 11. RMS of our estimated some QZSS receivers DCB with respect to the products provided by DLR and CAS. Subplot (a) C1X-C2X, (b) C1X-C5X, (c) C1C-C2L, (d) C1C-C5Q.

Table 7
Statistics for RMS of some receivers DCB respect to DLR and CAS (ns).

Type	CAS	DLR
C1X-C2X	0.80	0.50
C1X-C5X	0.98	0.57
C1C-C2L	1.15	0.70
C1C-C5Q	1.37	0.75
Mean	1.07	0.63

some receivers DCB is about 0.63 and 1.07 ns, with respect to DLR and CAS, respectively.

4. Conclusions

As an important error source in GNSS PPP and ionospheric modeling, the DCB needs to be estimated accurately. In this paper, the DCB of QZSS is estimated by adopting the global ionosphere modeling method based on QZSS/GPS combined observations from MGEX. The performance of QZSS satellite and receiver DCB is analyzed with observations during the period of DOY 275–364, 2018. In order to verify the method, the GIM provided by CODE is used as a reference, the mean Bias is about1.5-TECu and the mean RMS is about 2.8TECu. Similarly, the GPS C1C-C2W DCB provided by DLR and CAS is used as a reference. Our estimated GPS C1C-C2W satellites DCB shows good agreement with DLR and CAS.

The performance of QZSS satellite and receiver DCB is analyzed with observations during the period of DOY 275–364, 2018. A good agreement between our estimated QZSS satellites DCB and the products of DLR and CAS is shown. The Bias and RMS of DCB with respect to DLR are mostly within 0.2 ns, and the values with respect to CAS are mostly less than 0.3 ns. The day-to-day fluctuation in the DCB time series is <0.5 ns in about 96% of the cases for all satellites. Moreover, the high-level stability of our estimated QZSS satellites DCB is shown, which is at the same level as that of DLR and CAS. However, the receiver DCB is a little less stable than satellite DCB, and their STDs are within 1.9 ns. Although the receiver DCBs of the same type station (receiver and antenna) are similar, the stability of the receiver is not significantly related to the type of receiver and antenna.

Declaration of Competing Interest

All authors declare that No conflict of interest exists.

Acknowledgements

This work was supported by the National Natural Science Foundation of China-German Science Foundation (NSFC-DFG) Project (Grant No. 41761134092), Startup Foundation for Introducing Talent of NUIST (Grant No. 2243141801036), Jiangsu Province Distinguished Professor Project (Grant No. R2018T20) and Open fund project of Hubei Research Center of Engineering and

Technology for bridge safety monitoring and equipment (Grant No. QLZX2014010). We also thank IGS for providing MGEX data and DLR/CAS for providing the DCB products. Special thanks to Dr. Xu Tang and Dr. Andres Calabia for their help in English writing.

References

Fan, L., Li, M., Wang, C., Shi, C., 2017. BeiDou satellite's differential code biases estimation based on uncombined precise point positioning with triple-frequency observable. Adv. Space Res. 59, 804–814. https://doi.org/10.1016/j.asr.2016.07.014.

Hauschild, A., Steigenberger, P., Rodriguez-Solano, C., 2011. Signal, orbit and attitude analysis of Japan's first QZSS satellite Michibiki. GPS Solutions 16, 127–133. https://doi.org/10.1007/s10291-011-0245-5.

Jin, R., Jin, S.G., Feng, G.P., 2012. M_DCB: Matlab code for estimating GNSS satellite and receiver differential code biases. Gps Solutions 16, 541–548. https://doi.org/10.1007/s10291-012-0279-3.

Jin, S.G., Jin, R., Li, D., 2016. Assessment of BeiDou differential code bias variations from multi-GNSS network observations. Ann. Geophys. 34, 259–269. https://doi.org/10.5194/angeo-34-259-2016.

Jin, S.G., Su, K., 2020. PPP models and performances from single- to quad-frequency BDS observations. Satellite Navigat. 1. https://doi.org/10.1186/s43020-020-00014-y.

Li, M., Yuan, Y., Wang, N., Li, Z., Li, Y., Huo, X., 2017a. Estimation and analysis of Galileo differential code biases. J. Geodesy 91, 279–293. https://doi.org/10.1007/s00190-016-0962-1.

Li, W. et al., 2017b. GPS and BeiDou differential code bias estimation using Fengyun-3C satellite onboard GNSS observations. Remote Sens. 9. https://doi.org/10.3390/rs9121239.

Li, W., Wang, G., Mi, J., Zhang, S., 2019a. Calibration errors in determining slant Total Electron Content (TEC) from multi-GNSS data. Adv. Space Res. 63, 1670–1680. https://doi.org/10.1016/j.asr.2018.11.020.

Li, X., Xie, W., Huang, J., Ma, T., Zhang, X., Yuan, Y., 2019b. Estimation and analysis of differential code biases for BDS3/BDS2 using iGMAS and MGEX observations. J. Geodesy 93, 419–435. https://doi.org/10.1007/s00190-018-1170-y.

Li, X. et al., 2019c. Galileo and QZSS precise orbit and clock determination using new satellite metadata. J. Geodesy 93, 1123–1136. https://doi.org/10.1007/s00190-019-01230-4.

Li, Z., Yuan, Y., Fan, L., Huo, X., Hsu, H., 2014. Determination of the differential code bias for current BDS satellites. IEEE Trans. Geosci. Remote Sens. 52, 3968–3979. https://doi.org/10.1109/tgrs.2013.2278545.

Li, Z., Yuan, Y., Li, H., Ou, J., Huo, X., 2012. Two-step method for the determination of the differential code biases of COMPASS satellites. J. Geodesy 86, 1059–1076. https://doi.org/10.1007/s00190-012-0565-4.

Lin, J., Yue, X., Zhao, S., 2014. Estimation and analysis of GPS satellite DCB based on LEO observations. GPS Solut. 20, 251–258. https://doi.org/10.1007/s10291-014-0433-1.

Liu, T., Zhang, B., Yuan, Y., Li, Z., Wang, N., 2019. Multi-GNSS triple-frequency differential code bias (DCB) determination with precise point positioning (PPP). J. Geodesy 93, 765–784. https://doi.org/10.1007/s00190-018-1194-3.

Montenbruck, O., Hauschild, A., Steigenberger, P., 2014a. Differential code bias estimation using multi-GNSS observations and global ionosphere maps. Navigation 61, 191–201. https://doi.org/10.1002/navi.64.

Montenbruck, O., Steigenberger, P., Khachikyan, R., Weber, G., Langley, R., Mervart, L., Hugentobler, U., 2014b. IGS-MGEX: preparing the ground for multi-constellation GNSS science. Inside GNSS 9, 42–49.

Montenbruck, O. et al., 2017. The Multi-GNSS Experiment (MGEX) of the International GNSS Service (IGS)–achievements, prospects and challenges. Adv. Space Res. 59, 1671–1697.

Odolinski, R., Teunissen, P.J.G., Odijk, D., 2014. Combined BDS, Galileo, QZSS and GPS single-frequency RTK. GPS Solut. 19, 151–163. https://doi.org/10.1007/s10291-014-0376-6.

Quan, Y., Lau, L., Roberts, G.W., Meng, X., 2015. Measurement signal quality assessment on all available and new signals of multi-GNSS (GPS, GLONASS, Galileo, BDS, and QZSS) with real data. J Navigat. 69, 313–334. https://doi.org/10.1017/s0373463315000624.

Sanz, J., Miguel Juan, J., Rovira-Garcia, A., González-Casado, G., 2017. GPS differential code biases determination: methodology and analysis. GPS Solutions 21, 1549–1561. https://doi.org/10.1007/s10291-017-0634-5.

Shi, C., Fan, L., Li, M., Liu, Z., Gu, S., Zhong, S., Song, W., 2015. An enhanced algorithm to estimate BDS satellite's differential code biases. J. Geodesy 90, 161–177. https://doi.org/10.1007/s00190-015-0863-8.

Wang, N., Yuan, Y., Li, Z., Montenbruck, O., Tan, B., 2016. Determination of differential code biases with multi-GNSS observations. J. Geodesy 90, 209–228. https://doi.org/10.1007/s00190-015-0867-4.

Xue, J., Song, S., Liao, X., Zhu, W., 2016a. Estimating and assessing Galileo navigation system satellite and receiver differential code biases using the ionospheric parameter and differential code bias joint estimation approach with multi-GNSS observations. Radio Sci. 51, 271–283. https://doi.org/10.1002/2015rs005797.

Xue, J., Song, S., Zhu, W., 2016b. Estimation of differential code biases for Beidou navigation system using multi-GNSS observations: How stable are the differential satellite and receiver code biases?. J. Geodesy 90, 309–321. https://doi.org/10.1007/s00190-015-0874-5.

Zhang, B., Ou, J., Yuan, Y., Li, Z., 2012. Extraction of line-of-sight ionospheric observables from GPS data using precise point positioning. Sci. China Earth Sci. 55, 1919–1928. https://doi.org/10.1007/s11430-012-4454-8.

Zhang, B., Teunissen, P.J.G., 2015. Characterization of multi-GNSS between-receiver differential code biases using zero and short baselines. Sci. Bull. 60, 1840–1849. https://doi.org/10.1007/s11434-015-0911-z.

Zhang, Q., Zhao, Q., 2018. Global Ionosphere mapping and differential code bias estimation during low and high solar activity periods with GIMAS software. Remote Sens. 10. https://doi.org/10.3390/rs10050705.

Zhang, X., Xie, W., Ren, X., Li, X., Zhang, K., Jiang, W., 2017. Influence of the GLONASS inter-frequency bias on differential code bias estimation and ionospheric modeling. GPS Solutions 21, 1355–1367. https://doi.org/10.1007/s10291-017-0618-5.

Zhang, Y., Kubo, N., Chen, J., Wang, H., Wang, J., 2018. Assessment of the contribution of QZSS combined GPS/BeiDou positioning in Asia-Pacific areas. In: China Satellite Navigation Conference (CSNC) 2018 Proceedings. Lecture Notes in Electrical Engineering. pp. 467-478. 10.1007/978-981-13-0005-9_37.